JOURNAL OF MATERIALS SCIENCE 21 (1986) 4443–4450

Characterization of microvoids in polyacrylonitrile-based carbon fibres

A. TAKAKU, M. SHIOYA
Department of Textile and Polymeric Materials, Tokyo Institute of Technology, O-okayama, Meguro-ku, Tokyo, Japan

The microvoids in PAN-based carbon fibres covering a wide range of crystallite size were measured by the method using small-angle X-ray scattering on fibre bundles, and the fractional content of voids and the parameters representing the cross-sectional size of voids perpendicular to the fibre axis were determined. The variation in the shape and size distribution of voids with crystallite thickness was considered by introducing an elliptical cross-section model and a cross-sectional size distribution model. The electron density distribution in the inside of a void was also considered. It is concluded that the electron density difference between a void and the solid surrounding the void is relatively larger in the periphery than in the inner part of a void, and that the electron density in the inner part of a void decreases with increasing crystallite thickness.

1. Introduction

The small-angle X-ray scattering pattern of polyacrylonitrile(PAN)-based carbon fibres shows a lobe-shaped streak along the equator [1]. The small-angle X-ray scattering contains both density variations due to voids and density fluctuations due to stacking disorder [2], but its predominant component is assumed to be due to the existence of voids that are elongated parallel to the fibre axis. By using small-angle scattering, Johnson and Tyson [3] have evaluated the Porod distance of heterogeneity and the specific internal surface of the microvoids in PAN-based carbon fibres in relation to carbonization temperature.

The small-angle X-ray scattering is often measured on an apparently isotropic specimen prepared by grinding carbon fibres into powder. However, carbon fibres are so brittle that changes in microstructure due to the grinding may easily occur [4].

The present authors [5] have reported previously a method which enables one to analyse the small-angle X-ray scattering from the voids in a unidirectionally aligned fibrous material, and have deduced the parameters characterizing microvoids, such as the cross-sectional area S_3, the radius of gyration R_3, the length l_2, and the width l_3. Among the parameters the width l_3 is of special interest, since the l_3 value is sensitive to the electron density variation in the periphery of voids. It will be possible, therefore, to discuss in a quantitative manner the state of the periphery of voids by considering the l_3 value in relation to the other parameters which are insensitive to the state of the periphery of voids.

In this paper the fractional content and size parameters of the microvoids in PAN-based carbon fibres are evaluated by the previously developed method applying small-angle X-ray scattering. Furthermore, the shape and size distribution of microvoids and the electron density distribution in the inside of voids are discussed by postulating appropriate models.

2. Materials

PAN-based carbon fibres of seven types, which cover a wide range of crystallite size, were collected from commercial sources and supplied for measurements. These carbon fibres were in the form of tow, comprised of 6000 to 12000 filaments varying between types. The representative characteristics of the carbon fibres are shown in Table I, where the tensile modulus and the tensile strength were determined on carbon fibre–epoxy resin composite strands.

3. Methods of measurement

3.1. Density

The density of carbon fibres was measured at 25° C by a sink/float method using a carbon tetrachloride–ethylene dibromide mixture.

3.2. Wide-angle X-ray diffraction

About 20000 filaments of the carbon fibres were aligned in parallel and were formed into a bundle of rectangular cross-section with a matched die by using a small amount of adhesive. The bundle was mounted on a metal plate having a window for X-ray irradiation and then placed in the X-ray path. The X-ray diffraction measurement was made with a Rigaku Denki diffractometer using pinhole collimation of Cu$K\alpha$ nickel-filtered radiation.

The diffraction intensity distribution of the (0 0 2) diffraction was measured along the equator by using a position-sensitive proportional counter (PSPC) with a height-limiting slit of 1.5 mm width. The sample-to-detector distance was fixed at 110 mm. The correction for the X-ray absorption by a specimen was made on

0022–2461/86 $03.00 + .12 © *1986 Chapman and Hall Ltd.*

TABLE I Representative characteristics of carbon fibres supplied for measurements

Sample	Density ($g\,cm^{-3}$)	Layer thickness (nm)	Tensile modulus (GPa)	Tensile strength (GPa)
LC15	1.816	1.49	202	2.94
LC16	1.824	1.61	243	2.77
LC17	1.798	1.65	227	3.58
LC19	1.793	1.93	269	2.68
LC32	1.750	3.22	311	2.09
LC48	1.841	4.83	394	1.38
LC53	1.890	5.27	333	1.67

the diffraction intensity as measured. The absorption of a specimen was obtained from the ratio of the aluminium diffraction intensities measured with and without setting the specimen in the aluminium-diffracted line. From the corrected diffraction intensity the air scattering was subtracted, and then the corrections for the polarization and atomic scattering factors were made on the resulting diffraction intensity.

The average crystallite dimension in the c direction (layer thickness, L_c) was calculated, using the Scherrer equation

$$L_c = \frac{0.9\lambda}{(\Delta 2\theta)\cos\theta_p} \quad (1)$$

where λ is the X-ray wavelength, $\Delta 2\theta$ the half-height width of the diffraction intensity distribution (measured in radians) and θ_p the Bragg angle of the (0 0 2) reflection peak.

3.3. Small-angle X-ray scattering

The small-angle X-ray scattering measurements were carried out on the same specimens used for the wide-angle X-ray diffraction measurements.

The incident X-ray beam was collimated by pinholes of 0.3 and 0.5 mm in diameter. The sample-to-detector distance was 360 mm. The equatorial scattering intensity was detected by a PSPC with a pulse height discriminator. No height-limiting slit was adopted. The measuring time was 1000 sec.

The scattering intensity curve of the carbon fibres was obtained as follows. First, the corrections for the X-ray absorption by the fibres and air were made on the scattering curve as measured for the specimen. From the corrected scattering curve for the specimen was subtracted the air scattering curve, on which the absorption by air was corrected. The resulting scattering curve was determined as the scattering curve of the carbon fibres.

The incident X-ray beam power was determined by comparing the observed and theoretically calculated scattering intensities of air [5]. The specimen thickness was calculated from the X-ray absorption of a specimen, the density of carbon fibres and the mass absorption coefficient of carbon.

The parameters characterizing the voids in carbon fibres were calculated according to the method previously reported [5].

In this method the geometrical conditions for measuring the scattering intensity are postulated as follows. The X-ray beam is incident on a fibre specimen perpendicularly to the fibre axis. The direction perpendicular both to the X-ray beam and to the fibre axis is defined as the x axis. The scattering intensity is scanned in parallel to the x axis, and the origin of the x axis is set at the intercept of the x axis with the centre line of the X-ray beam. The scattering intensity $I(x)$ represents the total scattering intensity which is obtained by integrating in the direction parallel to the fibre axis the scattering intensity distribution at a distance x. Hence, $I(x)$ has the dimensions of counts per unit length. The sample-to-detector distance, D, is assumed to be constant. These geomerical conditions can be realized when measuring the equatorial small-angle scattering intensity by a PSPC without using a height-limiting slit.

The volume fraction of voids, v, is given as

$$v = \frac{2\pi m^2 c^4}{e^4\lambda^3(\Delta\varrho)^2 DtAI_0}\int_0^\infty I(x)\,x\,dx \quad (2)$$

where $\Delta\varrho$ is the electron density difference between the voids and the solid, m the electron mass, c the velocity of light, e the elementary electric charge, t the specimen thickness and AI_0 the incident X-ray beam flux.

Define l_2 as the average length of a segment which is cut by the contours of a void from a straight line being perpendicular to the fibre axis and passing through an arbitrary point in the void. The length of a void, l_2, is calculated by the equation

$$l_2 = \frac{\lambda D}{\pi}\frac{\int_0^\infty I(x)\,dx}{\int_0^\infty I(x)\,x\,dx} \quad (3)$$

The small-angle X-ray scattering intensity distribution at lower angles is represented as

$$\ln I(x) = -\frac{2\pi^2 R_3^2}{\lambda^2 D^2}x^2 + \ln S_3 + \ln\left(\frac{2\pi}{\lambda^2 D^2}\int_0^\infty I(x)\,x\,dx\right) \quad (4)$$

In the above equation, S_3 expresses the average area of a cross-section of a void, where the cross-section is perpendicular to the fibre axis and includes an arbitrary point in the void. R_3^2 represents the average of the squared radius of gyration of that cross-section of a void, where the average is taken by weighting the squared radius of gyration with the cross-sectional area. The plot of $(x^2, \ln I(x))$ at smaller values of x may be approximated by a straight line. From the intercept and slope of this straight line the values of S_3 and R_3 are determined by Equation 4.

The intensity distribution at higher angles may be represented as

$$[I(x)]^{-2/3} = \left[\int_0^\infty I(x)\,x\,dx\right]^{-2/3} \times\left[\left(\frac{\lambda D}{2\pi l_3}\right)^{4/3} + \left(\frac{2\pi l_3}{\lambda D}\right)^{2/3}x^2\right] \quad (5)$$

where l_3 is the average length of a segment defined by the contours of a void from an arbitrary straight line perpendicular to the fibre axis, and is calculated from

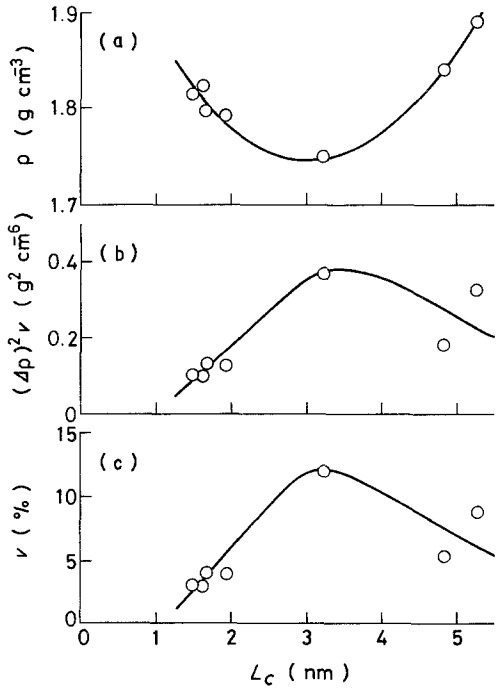

Figure 1 (a) Fibre density, (b) void content parameter $(\Delta\varrho)^2 v$ and (c) volume fraction of voids plotted against layer thickness L_c for various types of carbon fibre.

the slope of a straight line approximating the plot of $(x^2, I(x)^{-2/3})$. The parameter l_3 is referred to as the width of a void.

The small-angle X-ray scattering intensities could be practically measurable in the 2θ range from a few minutes of arc to a few degrees. The integrations of the scattering intensities in Equations 2 to 5, therefore, were performed on the extended intensity curves obtained by extrapolating the linear portion of the $(x^2, \ln I(x))$ plot to $x \to 0$ and that of $(x^2, I(x)^{-2/3})$ plot to $x \to \infty$.

4. Experimental results

For the carbon fibres of various types the density ϱ, the void content parameter $(\Delta\varrho)^2 v$ and the volume fraction of voids v, are shown as functions of the layer thickness L_c in Figs 1a, b and c, respectively. In calculating the volume fraction of voids the electron density difference was approximated by the average electron density calculated from the fibre density. The density shows a minimum at a layer thickness of about 3 nm, while the void content indices $(\Delta\varrho)^2 v$ and v seem to take maxima at the same layer thickness.

In Figs 2a, b, c and d the size parameters of voids, S_3, R_3, l_2 and l_3, are plotted against the layer thickness. It can be said that the average size of voids in the fibre cross-section perpendicular to the fibre axis becomes larger with increasing layer thickness.

5. Discussion

5.1. Cross-section models of voids

The size parameters S_3, R_3, l_2 and l_3 can be deduced without postulating any assumptions about the shape and size distribution of voids. However, the parameters do not provide information on the shape and size distribution of the cross-section of voids. Such information cannot normally be deduced in a straightforward manner from small-angle X-ray scattering alone without making some assumptions about the geometrical features of voids. Hence, in this paper, models for the shape and size distribution of voids are introduced. The experimental results of small-angle scattering are analysed on the basis of the models, and the nature of voids in PAN-based carbon fibres is considered.

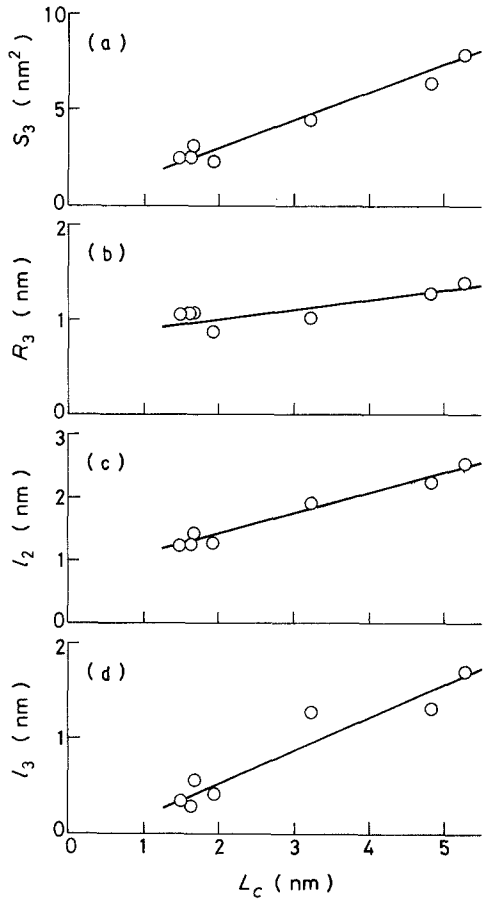

Figure 2 Plots of void-size parameters against layer thickness L_c: (a) cross-sectional area S_3, (b) radius of gyration R_3, (c) length l_2 and (d) width l_3.

5.1.1. Elliptical cross-section model

Assume that all the cross-sections of the voids are elliptical and the same in size perpendicular to the fibre axis, and that the electron density distribution in the cross-section is uniform and constant. The major and minor axes of the elliptical cross-section are designated as μr_e and r_e, respectively. Then, the parameters S_3, R_3, l_2 and l_3 for this model are given from Equations A9, A10, A11 and A12 in the Appendix as follows:

$$S_3 = \pi\mu r_e^2 \tag{6}$$

$$R_3 = \tfrac{1}{2}(\mu^2 + 1)^{1/2} r_e \tag{7}$$

$$l_2 = \frac{32}{3\pi^2} F[(1 - \mu^{-2})^{1/2}] r_e \tag{8}$$

$$l_3 = \frac{\pi^2}{4} \frac{r_e}{E[(1 - \mu^{-2})^{1/2}]} \tag{9}$$

where $F(x)$ and $E(x)$ stand for the complete elliptic integrals of the first and second kinds, respectively.

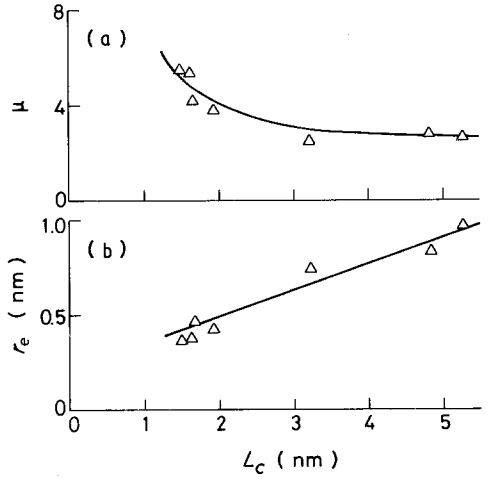

Figure 3 Plots of (a) aspect ratio and (b) minor-axis length, calculated from elliptical cross-section model, against layer thickness L_c.

The values of μ and r_e, which were calculated by using Equations 6 and 7 with the values of S_3 and R_3, are plotted against the layer thickness L_c in Figs 3a and b. With increasing L_c the axial length r_e increases almost linearly, while the aspect ratio, μ, decreases with increasing L_c up to about 3 nm and shows a constant value at larger values of L_c than about 3 nm.

In Fig. 4 the values of l_2 calculated from Equation 8 with the values of μ and r_e are compared with those experimentally obtained. As is found in Fig. 4, the calculated values are in good agreement with the experimental values.

5.1.2. Cross-sectional size distribution model

Assume that all the voids in carbon fibres have circular cross-sections perpendicular to the fibre axis and that the electron density distribution in the cross-sections is uniform and constant. Designate the radius of the cross-section of a void by r, and assume that the distribution function of the radius r is represented as follows:

$$f(r) = \frac{\alpha}{\Gamma[(\beta + 1)/\alpha] r_0} \left(\frac{r}{r_0}\right)^{\beta} \exp\left[-\left(\frac{r}{r_0}\right)^{\alpha}\right] \quad (\alpha > 0, \quad \beta > -1) \tag{10}$$

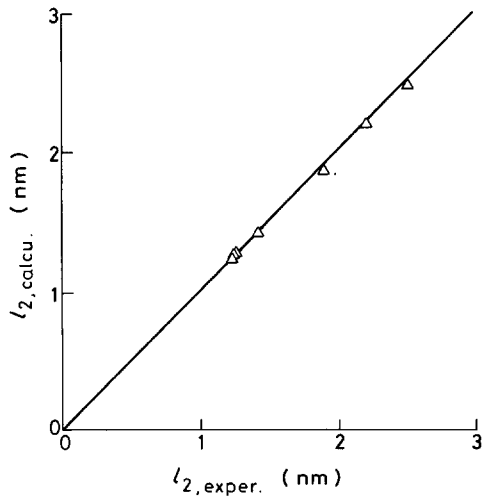

Figure 4 Comparison between the l_2 value calculated from the elliptical cross-section model and the l_2 value obtained experimentally.

TABLE II Distribution parameters of radii of void cross-sections

Sample	α	r_0 (nm)
LC15	0.69	0.0562
LC16	0.70	0.0605
LC17	0.89	0.159
LC19	1.02	0.202
LC32	2.16	0.901
LC48	1.66	0.815
LC53	1.88	1.05

where α, β and r_0 are the constants which will be determined experimentally, and Γ denotes a gamma function. This model will be referred to as the cross-sectional size distribution model. The parameters S_3, R_3, l_2 and l_3 for this model are given from Equations A13, A14, A15 and A16 in the Appendix as

$$S_3 = \pi r_0^2 \frac{\Gamma[(\beta + 5)/\alpha]}{\Gamma[(\beta + 3)/\alpha]} \tag{11}$$

$$R_3^2 = \tfrac{1}{2} r_0^2 \frac{\Gamma[(\beta + 7)/\alpha]}{\Gamma[(\beta + 5)/\alpha]} \tag{12}$$

$$l_2 = \frac{16}{3\pi} r_0 \frac{\Gamma[(\beta + 4)/\alpha]}{\Gamma[(\beta + 3)/\alpha]} \tag{13}$$

$$l_3 = \frac{\pi}{2} r_0 \frac{\Gamma[(\beta + 3)/\alpha]}{\Gamma[(\beta + 2)/\alpha]} \tag{14}$$

Equation 10 represents a Maxwellian distribution when $\alpha = 2$. For a Maxwellian distribution the parameters S_3 and R_3 are written from Equations 11 and 12 as

$$S_3 = \pi r_0^2 \frac{\beta + 3}{2} \tag{15}$$

$$R_3^2 = \tfrac{1}{2} r_0^2 \frac{\beta + 5}{2} \tag{16}$$

Since $\beta > -1$, the following relation should be satisfied:

$$2\pi > S_3/R_3^2 > \pi \tag{17}$$

It was found from the experimental results in Fig. 2 that Equation 17 cannot hold for carbon fibres having layer thicknesses smaller than about 3 nm. Therefore, by determining that $\beta = 1$, and by assuming α and r_0 as adjustable parameters, the values of these adjustable parameters were determined by computer simulation, using Equations 11 and 12 with the values of S_3 and R_3. The results obtained are listed in Table II. Fig. 5 shows the cross-sectional size distribution curves thus determined.

The values of l_2 calculated from Equation 13 with the values of α and r_0 are compared with those experimentally obtained in Fig. 6. In Fig. 6 the calculated values are in good agreement with the experimental values.

As is indicated from Figs 4 and 6, both the elliptical cross-section model and the cross-sectional size distribution model can be applicable to the experimental results of small-angle X-ray scattering. In other words, it is difficult to assess from small-angle X-ray scattering alone, which model is more appropriate for describing the features of voids in the cabon fibres.

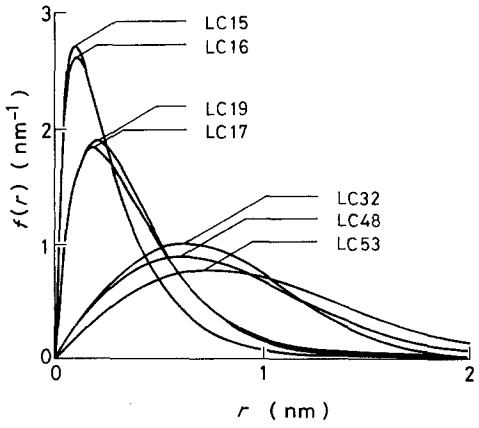

Figure 5 Distribution $f(r)$ of the radius r of void cross-sections, calculated from cross-sectional size distribution model, for various carbon fibres indicated.

5.2. Electron density

The l_3 value can be calculated on the basis of the elliptical cross-section model or the cross-sectional size distribution model, using Equation 9 with the values μ and r_e in Fig. 3 or Equation 14 with the values α and r_0 in Table II, respectively. The results of calculation are shown in Fig. 7 as the ratio of the experimental value against the calculated value of l_3, plotted against the layer thickness. It is noted in Fig. 7 that the l_3 values calculated from the two models for a particular sample are almost identical, and that the l_3 value experimentally obtained is always smaller than the calculated one. The experimental value of l_3 tends to approach the calculated value with increasing layer thickness.

The major reason for the discrepancy between the experimental and calculated values of l_3 is considered to be due to the fact that the parameter l_3 concerns, in the procedure deducing it from the small-angle X-ray scattering, the first slope of the autocorrelation of the electron density function for the void cross-sections. The electron density function may have a gradual variation in the cross-section of a void. The experimental value of l_3, therefore, will change with the electron density distribution in the periphery of a void.

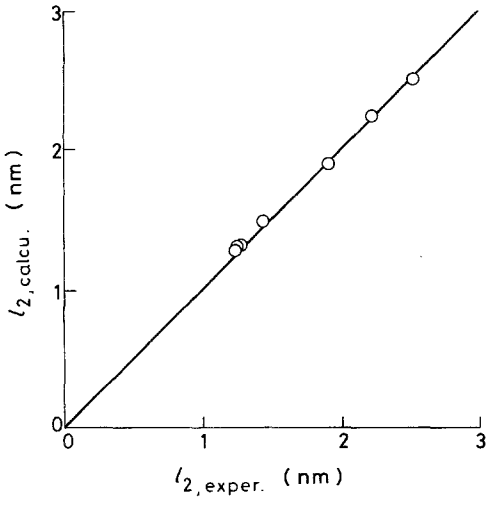

Figure 6 Comparison between the l_2 value calculated from the cross-sectional size distribution model and the l_2 value obtained experimentally.

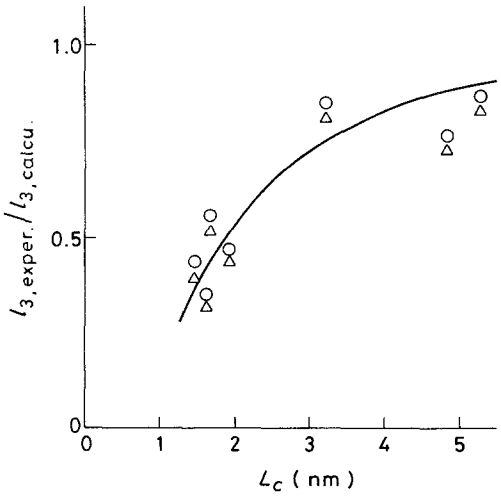

Figure 7 The ratio of the experimental value l_3 to the calculated value l_3 plotted against layer thickness L_c. The l_3 values are calculated from (△) the elliptical cross-section model and (○) the cross-sectional size distribution model.

Consider a void having a circular cross-section perpendicular to the fibre axis, where the radius of the cross-section is denoted as r_c. Designate as l_3' the l_3 value obtained when the electron density distribution in the cross-section of a void is uniform and constant. Then l_3' is given from Equation A16 in the Appendix as

$$l_3' = \frac{\pi}{2} r_c \tag{18}$$

The value l_3' may be considered to correspond approximately to the l_3 value which is calculated from the values S_3 and R_3. On the other hand, when the electron density difference in a void has a smooth fluctuation $\Delta\varrho(z)$, by designating as l_3'' the l_3 value obtained on this occasion, the value l_3'' is represented from Equation A17 in the Appendix as

$$l_3'' = \frac{\iint [\Delta\varrho(z)]^2 \, dz_1 \, dz_2}{2[\Delta\varrho(r_c)]^2 r_c} \tag{19}$$

Hence, from the comparison of Equations 18 and 19 it is known that the relation $l_3' > l_3''$ is valid when $|\Delta\varrho(r_c)| > |\Delta\varrho(z)|$ for $r_c > |z|$. That is, the fact that the experimental values of l_3 being always smaller than the calculated ones from Equations 9 and 14 implies that the electron density difference is smaller in the inner part of a void than in the periphery of the void.

For simplicity, represent $\Delta\varrho(z)$ as

$$\Delta\varrho(z) = \Delta\varrho(r_c)\left[(1 - \phi)\left(\frac{z}{r_c}\right)^2 + \phi\right] \tag{20}$$

From Equations 18 and 19

$$\frac{l_3''}{l_3'} = \tfrac{1}{3}(\phi^2 + \phi + 1) \tag{21}$$

The value of ϕ can be deduced by assuming that the ratio l_3''/l_3' is equivalent to the ratio of the l_3 value experimentally obtained to that calculated from the elliptical cross-section model or from the cross-sectional size distribution model. Fig. 8 shows the electron density distribution in the cross-section of a

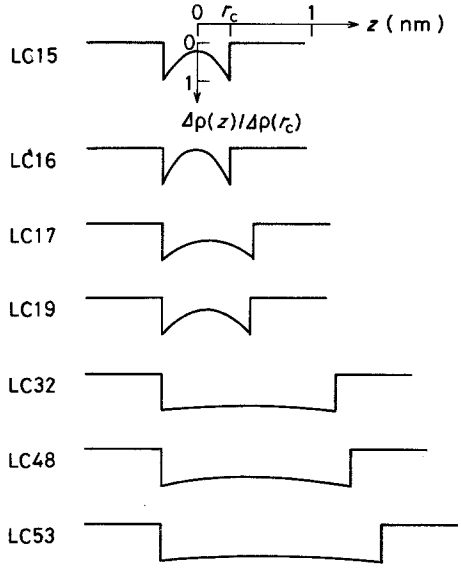

Figure 8 Electron density distribution $\Delta\varrho(z)/\Delta\varrho(r_c)$ in the void cross-section for the various carbon fibres indicated.

void, which is calculated by using the values ϕ and the average radius obtained for the cross-sectional size distribution model.

5.3. Scattering of size

In the S_3, R_3 and l_2 values, larger cross-sections of the voids in a fibre may be emphasized, since the averages for these parameters are taken over all the points in voids. It will be adequate, therefore, to adopt as a size parameter corresponding to a visual image of the voids the l_3 value calculated with two from the S_3, R_3 and l_2 values, rather than a value experimentally obtained.

According to the elliptical cross-section model, by using S_3 and R_3 the coefficient of variation of l_3, σ_3/l_3, is represented as

$$\left(\frac{\sigma_3}{l_3}\right)^2 = \frac{128}{3\pi^4} F[(1-\mu^{-2})^{1/2}]E[(1-\mu^{-2})^{1/2}] - 1 \tag{22}$$

Similarly, for the cross-sectional size distribution model the coefficient of variation is given as

$$\left(\frac{\sigma_3}{l_3}\right)^2 = \frac{32}{3\pi^2} \frac{\Gamma[(\beta+4)/\alpha]\,\Gamma[(\beta+2)/\alpha]}{\{\Gamma[(\beta+3)/\alpha]\}^2} - 1 \tag{23}$$

The values of l_3 and σ_3/l_3, which were calculated from Equations 9 and 22 with the values of μ and r_e in Fig. 3 and from Equations 14 and 23 with the values of α and r_0 in Table II, are plotted against the layer thickness L_c in Fig. 9. With increasing layer thickness the cross-sectional size of voids becomes larger, but its coefficient of variation decreases rapidly and shows almost a constant value of 0.5 at layer thicknesses larger than about 3 nm.

6. Conclusions

The microvoids in PAN-based carbon fibres covering a wide range of layer thickness are investigated by measuring the absolute small-angle X-ray scattering

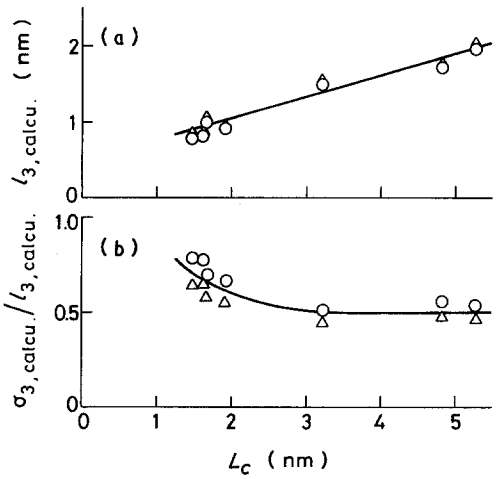

Figure 9 Plots of (a) l_3 and (b) its coefficient of variation σ_3/l_3 against layer thickness L_c: calculated (△) from elliptical cross-section model and (○) from cross-sectional size distribution model.

from fibre bundles. The small-angle scattering was analysed by the method previously reported, and the fractional content of voids and the parameters representing the void cross-sectional size perpendicular to the fibre axis were determined. The void size tends to be large for the fibres having larger layer thicknesses. On the other hand, the void content takes a maximum at a layer thickness of about 3 nm. The density of carbon fibres forms a minimum at the same layer thickness.

In order to consider the shape and size distribution of voids in the fibre cross-section, the elliptical cross-section model and the size distribution model (assuming a circular cross-sectional shape of voids) have been introduced. The elliptical cross-section model has shown that the cross-sections of voids in the fibres having smaller layer thicknesses are ellipses of comparatively larger aspect ratios, and that the aspect ratio becomes smaller with increasing layer thickness. If the cross-section of voids is assumed to be circular, then the distribution of radii of voids can be represented by the distribution function

$$f(r) = \frac{\alpha}{\Gamma(2/\alpha)r_0}\left(\frac{r}{r_0}\right)\exp\left[-\left(\frac{r}{r_0}\right)^{\alpha}\right]$$

where α and r_0 are adjustable parameters. This distribution function is applicable to PAN-based carbon fibres covering a wide range of layer thickness. These two models can be applied to the experimental results of the small-angle scattering. However, from the small-angle scattering experiment alone it is difficult to evaluate which model is more appropriate for describing the voids in the carbon fibres. Both models have indicated that the coefficient of variation of the void width is larger for the fibres of smaller layer thicknesses and decreases with increasing layer thickness.

The analysis of the void width l_3 makes it possible to consider the electron density distribution in the inside of a void. It is concluded that the electron density difference between a void and the solid surrounding the void is relatively larger in the periphery than in the inner part of a void, and that the electron density in the inner part of a void decreases with increasing layer thickness.

Appendix

A.1. Definitions of size parameters

Designate the real-space vectors by z and a. The components of z and a, which are parallel to the direction in which the scattering intensity is scanned, are represented by z_1 and a_1, respectively. The components parallel to the incident X-ray beam are represented by z_2 and a_2, and those parallel to the fibre axis are denoted by z_3 and a_3. dv_z is the volume element at a position z. In the present experimental geometry, the observed scattering intensity does not depend on the correlation of the electron density distribution in the direction of the fibre axis. That is, if we divide the voids into infinitely thin sections perpendicularly to the fibre axis, the assembly of these sections give the same scattering intensity distribution as that from the original voids. Therefore, by denoting $\Delta\varrho_k(z)$ as the electron density difference between the kth section of voids and the solid, the definitions of the parameters S_3, R_3, l_2 and l_3 [5] are expressed as follows:

$$S_3 = \frac{\sum_k \int \left[\iint \Delta\varrho_k(z)\ dz_1\, dz_2 \right] \Delta\varrho_k(z)\, dv_z}{\sum_k \int [\Delta\varrho_k(z)]^2\, dv_z} \tag{A1}$$

$$R_3^2 = \frac{\sum_k \int \left[\iint \Delta\varrho_k(\boldsymbol{g}_k + \boldsymbol{a})|\boldsymbol{a}|^2\, da_1\, da_2 \right] \Delta\varrho_k(z)\, dv_z}{\sum_k \int \left[\iint \Delta\varrho_k(z)\, dz_1\, dz_2 \right] \Delta\varrho_k(z)\, dv_z} \tag{A2}$$

$$l_2 = \frac{\sum_k \int \left[\int \Delta\varrho_k(z)\, dz_2 \right] \Delta\varrho_k(z)\, dv_z}{\sum_k \int [\Delta\varrho_k(z)]^2\, dv_z} \tag{A3}$$

$$l_3 = \left[-\lim_{a_1 \to 0} \frac{d}{da_1} \times \frac{\sum_k \int \Delta\varrho_k(z)\, \Delta\varrho_k(z_1 - a_1, z_2, z_3)\, dv_z}{\sum_k \int [\Delta\varrho_k(z)]^2\, dv_z} \right]^{-1} \tag{A4}$$

where $\boldsymbol{g}_k$ is the centre of gravity of the kth section, and $a_3 = 0$. In the above expressions, Σ can be replaced by $N\langle\ \rangle$, where $\langle\ \rangle$ is a number average with regard to all the thin sections, and N a total number of the thin sections involved in the voids. Thus, Equations A1, A2, A3 and A4 are rewritten respectively as

$$S_3 = \frac{N\left\langle \left[\iint \Delta\varrho_k(z)\, dz_1\, dz_2 \right]^2 \right\rangle \Delta z_3}{N\left\langle \iint [\Delta\varrho_k(z)]^2\, dz_1\, dz_2 \right\rangle \Delta z_3} \tag{A5}$$

$$R_3^2 = \frac{N\left\langle \left[\iint \Delta\varrho_k(\boldsymbol{g}_k + \boldsymbol{a})|\boldsymbol{a}|^2\, da_1\, da_2 \right] \left[\iint \Delta\varrho_k(z)\, dz_1\, dz_2 \right] \right\rangle \Delta z_3}{N\left\langle \left[\iint \Delta\varrho_k(z)\, dz_1\, dz_2 \right]^2 \right\rangle \Delta z_3} \tag{A6}$$

$$l_2 = \frac{N\left\langle \int \left[\int \Delta\varrho_k(z)\, dz_2 \right]^2 dz_1 \right\rangle \Delta z_3}{N\left\langle \iint [\Delta\varrho_k(z)]^2\, dz_1\, dz_2 \right\rangle \Delta z_3} \tag{A7}$$

$$l_3 = \left[-\lim_{a_1 \to 0} \frac{d}{da_1} \frac{N\left\langle \iint \Delta\varrho_k(z)\, \Delta\varrho_k(z_1 - a_1, z_2)\, dz_1\, dz_2 \right\rangle \Delta z_3}{N\left\langle \iint [\Delta\varrho_k(z)]^2\, dz_1\, dz_2 \right\rangle \Delta z_3} \right]^{-1} \tag{A8}$$

where Δz_3 is the thickness of a thin section, and z, $\boldsymbol{g}_k$ and $\boldsymbol{a}$ are the two-dimensional vectors.

A.2. Elliptical cross-section model

Consider that all the cross-sections of the voids are elliptical in planes perpendicular to the fibre axis and that the electron density distribution in the cross-sections is uniform and constant. Assuming that the voids are distributed with cylindrical symmetry around the fibre axis, and denoting the major and minor axes of the kth elliptical cross-section as $\mu_k r_k$ and r_k, respectively, we obtain

$$S_3 = \pi \frac{\langle \mu_k^2 r_k^4 \rangle}{\langle \mu_k r_k^2 \rangle} \tag{A9}$$

$$R_3^2 = \frac{1}{4} \frac{\langle (\mu_k^2 + 1) \mu_k^2 r_k^6 \rangle}{\langle \mu_k^2 r_k^4 \rangle} \tag{A10}$$

$$l_2 = \frac{32}{3\pi^2} \frac{\langle \mu_k F[(1 - \mu_k^{-2})^{1/2}] r_k^3 \rangle}{\langle \mu_k r_k^2 \rangle} \tag{A11}$$

$$l_3 = \frac{\pi^2}{4} \frac{\langle \mu_k r_k^2 \rangle}{\langle \mu_k E[(1 - \mu_k^{-2})^{1/2}] r_k \rangle} \tag{A12}$$

Replacing μ_k and r_k in the above equations by μ and r_e, respectively, leads to Equations 6, 7, 8 and 9.

A.3. Cross-sectional size distribution model

Consider that all the cross-sections of the voids are circular but different in size perpendicular to the fibre axis. Assume that the distribution of the radius r of the cross-sections is represented by Equation 10, and that the electron density distribution in the cross-sections is uniform and constant. Then, putting $\mu_k = 1$ and $r_k = r$ in Equations A9, A10, A11 and A12 leads to

$$S_3 = \pi \frac{\langle r^4 \rangle}{\langle r^2 \rangle} \tag{A13}$$

$$R_3^2 = \frac{1}{2} \frac{\langle r^6 \rangle}{\langle r^4 \rangle} \tag{A14}$$

$$l_2 = \frac{16}{3\pi}\frac{\langle r^3\rangle}{\langle r^2\rangle} \quad \text{(A15)}$$

$$l_3 = \frac{\pi}{2}\frac{\langle r^2\rangle}{\langle r\rangle} \quad \text{(A16)}$$

By using Equation 10, Equations A13, A14, A15 and A16 are rewritten as Equations 11, 12, 13 and 14, respectively.

A.4. Electron density distribution in a void

Assume that all the cross-sections of the voids are circular and the same in radius r_c perpendicular to the fibre axis, and represent the difference in electron density between the void and the solid by $\Delta\varrho(z)$ as a function of the distance z from the centre of the void cross-section. Then

$$\lim_{a_1\to 0}\frac{\mathrm{d}}{\mathrm{d}a_1}\iint \Delta\varrho(z)\,\Delta\varrho(z_1 - a_1, z_2)\,\mathrm{d}z_1\,\mathrm{d}z_2$$

$$= \lim_{a_1\to 0}\frac{\mathrm{d}}{\mathrm{d}a_1} 4\int_{z_1=a_1/2}^{r_c} \times \int_{z_2=0}^{(r_c^2-z_1^2)^{1/2}} \Delta\varrho(z)\,\Delta\varrho(z_1 - a_1, z_2)\,\mathrm{d}z_2\,\mathrm{d}z_1$$

$$= -2\int_0^{r_c}\{\Delta\varrho[(r_c^2 - z_2^2)^{1/2}, z_2]\}^2\,\mathrm{d}z_2 \quad \text{(A17)}$$

Arranging Equation A8 by using Equation A17 gives Equation 19.

References

1. D. J. JOHNSON and C. N. TYSON, *Br. J. Appl. Phys. (J. Phys. D)* **2** (1969) 787.
2. R. PERRET and W. RULAND, *J. Appl. Cryst.* **3** (1970) 525.
3. D. J. JOHNSON and C. N. TYSON, *J. Phys. D; Appl. Phys.* **3** (1970) 526.
4. R. PERRET and W. RULAND, *J. Appl. Cryst.* **2** (1969) 209.
5. M. SHIOYA and A. TAKAKU, *J. Appl. Phys.* **58** (1985) 4074.

Received 21 February
and accepted 28 April 1986